Intramolecular Optical Electron Transfer in Mixed-Valent Dinuclear Iron−Ruthenium Complexes Featuring a 1,4-Diethynylaryl Spacer

Nicolas Gauthier,[†] Céline Olivier,[†] Stéphane Rigaut,*[,†] Daniel Touchard,[†] Thierry Roisnel,[†,‡] Mark G. Humphrey,*[,§] and Frédéric Paul*[,†,‡]

Université de Rennes 1, Sciences Chimiques de Rennes, Campus de Beaulieu, 35042 Rennes Cedex, France, CNRS (UMR 6226), Université de Rennes 1, Sciences Chimiques de Rennes, Campus de Beaulieu, 35042 Rennes Cedex, France, and Department of Chemistry, Australian National University, Canberra, Australian Capital Territory 0200, Australia

Received June 14, 2007

The ground-state electronic structure and the lowest-lying excited states of the cationic mixed-valent dinuclear complexes [(η^2-dppe)(η^5-C_5Me_5)Fe[C≡C-1,4-(C_6H_4)C≡C]Ru(η^2-dppe)$_2$(X)][PF_6] (X = Cl, **2**; X = C≡C(4-$C_6H_4NO_2$), **5**) are discussed, with particular emphasis on the photoinduced intramolecular electron transfer between the ruthenium and iron centers. The location and intensities of the low-lying absorptions exhibited in the near-infrared (near-IR) range by these heterodinuclear mixed-valent (MV) complexes correlate with predictions based on the Hush model, strongly suggesting that they correspond to intervalence charge-transfer (IVCT) bands.

Introduction

In the field of mixed-valent (MV) complexes, dinuclear compounds featuring a carbon-rich bridge directly linked to the redox centers by metal–carbon bonds have attracted particular attention as a potentially interesting class of compounds for various applications in the field of molecular-scale electronics.[1–3] The classical Hush treatment used to rationalize the electron transfer of purely inorganic MV complexes has been successfully extended to symmetrical representatives of this new class of carbon-rich organometallic MV complexes such as **1**[PF_6],[4–6] but this simple model has seldom been applied to unsymmetrical representatives.[7,8]

Some of us recently reported a new redox family of heterometallic iron/ruthenium aryl acetylide complexes (**2**/**2**$^+$/**2**$^{2+}$ in Chart 1) designed for switching the third-order nonlinear optical (NLO) activity between three redox states.[9] The successful use of this redox family for such a purpose rests on the kinetic stability and on the widely differing optical properties of the various redox states.[10,11] In order to gain a better understanding of the molecular origin of the NLO properties of **2**/**2**[PF_6]/**2**[PF_6]$_2$, we have started to investigate more closely the lowest-lying excited states of each redox congener. In contrast to what might have been anticipated from previous studies on related complexes,[10,12–15] our investigations on the cationic complex **2**[PF_6] strongly suggest that the low-lying intense absorption at 1124 nm corresponds to a Ru−Fe intervalence charge-transfer (IVCT) band. This result is of particular interest in the context of recent investigations of related symmetric homodinuclear ruthenium MV complexes such as **3**[PF_6] and **4**[PF_6], where the nature of the most intense low-lying absorptions has also been discussed.[13,14,16] With the MV complex **3**[PF_6], the classical Hush model was unable to rationalize the spectral features of the low-energy absorption near 1500 nm that was believed to be an IVCT band.[13,16] With

[†] Sciences Chimiques de Rennes, Université de Rennes 1.
[‡] CNRS (UMR 6226), Université de Rennes 1.
[§] Australian National University.

(1) (a) Kim, B.; Beebe, J. M.; Olivier, C.; Rigaut, S.; Touchard, D.; Kushmerick, J. G.; Zhu, X.-Y.; Frisbie, C. D. *J. Phys. Chem. C* **2007**, *111*, 7521–7526. (b) Rigaut, S.; Touchard, D.; Dixneuf, P. H. In *Redox Systems Under Nano-space Control*; Hirao, T., Ed.; Springer: Heidelberg, Germany, 2006. (c) Low, P. J. *Dalton Trans.* **2005**, 2821–2824. (d) Long, N. J.; Williams, C. K. *Angew. Chem., Int. Ed. Engl.* **2003**, *42*, 2586–2617. (e) Paul, F.; Lapinte, C. In *Unusual Structures and Physical Properties in Organometallic Chemistry*; Gielen, M., Willem, R., Wrackmeyer, B., Eds.; Wiley: San Francisco, 2002; pp 219–295.

(2) Ceccon, A.; Santi, S.; Orian, L.; Bisello, A. *Coord. Chem. Rev.* **2004**, *248*, 683–724.

(3) Paul, F.; Lapinte, C. *Coord. Chem. Rev.* **1998**, *178/180*, 427–505.

(4) Ibn Ghazala, S.; Paul, F.; Toupet, L.; Roisnel, T.; Hapiot, P.; Lapinte, C. *J. Am. Chem. Soc.* **2006**, *128*, 2463–2476.

(5) Crutchley, R. J. *Adv. Inorg. Chem.* **1994**, *41*, 273–325.

(6) (a) Launay, J.-P.; Coudret, C. In *Electron Transfer in Chemistry*; Balzani, V., de Silva, A. P., Eds.; Wiley-VCH: Weinheim, Germany, 2000; Vol. 5, pp 3–47. (b) Launay, J.-P. *Chem. Soc. Rev.* **2001**, *30*, 386–397.

(7) (a) Coat, F.; Guillevic, M.-A.; Toupet, L.; Paul, F.; Lapinte, C. *Organometallics* **1997**, *16*, 5988–5998. (b) Paul, F.; Meyer, W.; Jiao, H.; Toupet, L.; Gladysz, J. A.; Lapinte, C. *J. Am. Chem. Soc.* **2000**, *122*, 9405–9414.

(8) Bruce, M. I.; Costuas, K.; Davin, T.; Ellis, B. J.; Halet, J.-F.; Lapinte, C.; Low, P. J.; Smith, M. E.; Skelton, B. W.; Toupet, L.; White, A. H. *Organometallics* **2005**, *24*, 3864–3881.

(9) Samoc, M.; Gauthier, N.; Cifuentes, M. P.; Paul, F.; Lapinte, C.; Humphrey, M. G. *Angew. Chem., Int. Ed.* **2006**, *45*, 7376–7379.

(10) Powell, C. E.; Cifuentes, M. P.; Morrall, J. P.; Stranger, R.; Humphrey, M. G.; Samoc, M.; Luther-Davies, B.; Heath, G. A. *J. Am. Chem. Soc.* **2003**, *125*, 602–610.

(11) Cifuentes, M. P.; Powell, C. E.; Morrall, J. P. L.; McDonagh, A. M.; Lucas, N. T.; Humphrey, M. G.; Samoc, M.; Houbrechts, S.; Asselberghs, I.; Clays, K.; Persoons, A.; Isoshima, T. *J. Am. Chem. Soc.* **2006**, *128*, 10819–10832.

(12) Paul, F.; Toupet, L.; Thépot, J.-Y.; Costuas, K.; Halet, J.-F.; Lapinte, C. *Organometallics* **2005**, *24*, 5464–5478.

(13) Klein, A.; Lavastre, O.; Fiedler, J. *Organometallics* **2006**, *25*, 635–643.

(14) Maurer, J.; Sarkar, B.; Schwederski, B.; Kaim, W.; Winter, R. F.; Zalis, S. *Organometallics* **2006**, *25*, 3701–3712.

(15) Rigaut, S.; Olivier, C.; Costuas, K.; Choua, S.; Fadhel, O.; Massue, J.; Turek, P.; Saillard, J.-Y.; Dixneuf, P. H.; Touchard, D. *J. Am. Chem. Soc.* **2006**, *128*, 5859–5876.

(16) Colbert, M. C. C.; Lewis, J.; Long, N. J.; Raithby, P. R.; Younus, M.; White, A. J. P.; Williams, D. J.; Payne, N. J.; Yellowlees, L.; Beljonne, D.; Chawdhury, N.; Friend, R. H. *Organometallics* **1998**, *17*, 3034–3043.

10.1021/om700584m CCC: $40.75
Publication on Web 02/27/2008

Chart 1. Selected Dinuclear MV Complexes and Redox Interconversions among 2, 2^+, and 2^{2+}

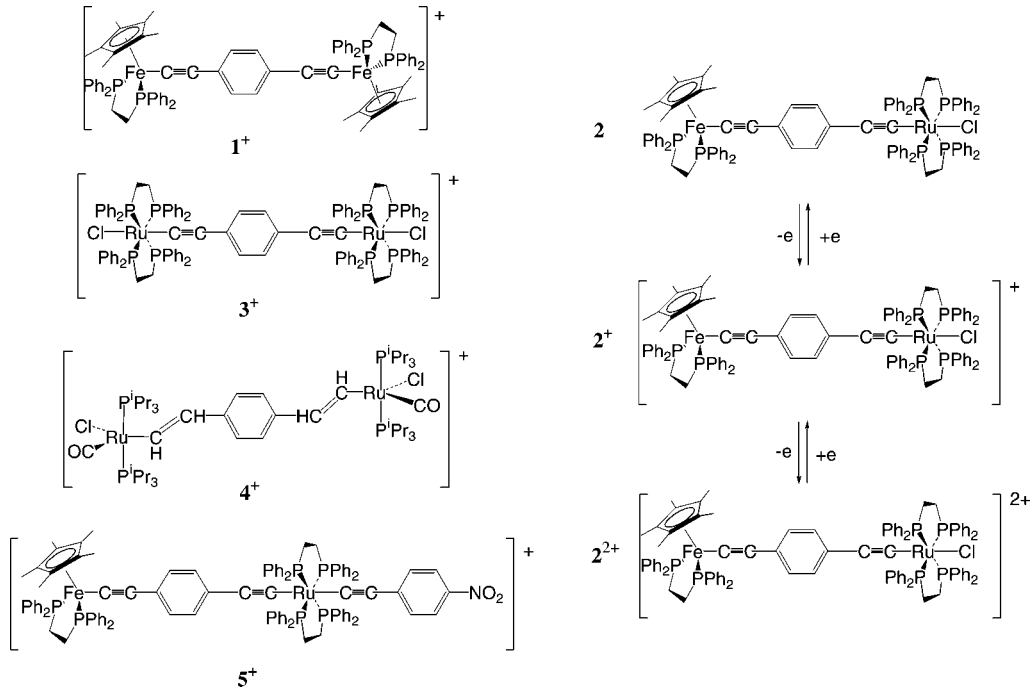

the MV complex **4**[PF_6], Winter and co-workers have proposed that the low-energy absorption is dominated by contributions from ligand-centered (LC) $\pi-\pi^*$ transitions rather than metal-to-metal charge-transfer transitions.[14] The current belief with these dinuclear carbon-rich MV complexes containing electron-rich ruthenium centers is that the low-lying intense transitions should not a priori be envisioned as metal-to-metal or intervalence charge-transfer (MMCT or IVCT) transitions.[17] More generally, the appropriateness of using the Hush model with such MV complexes exhibiting a sizable delocalization of the unpaired electron in the ground state (GS) has been questioned.[8,13] We report in this contribution the synthesis of **2**[PF_6] and of a MV analogue containing a 4-nitrophenyl alkynyl ligand in place of the chloride ligand (**5**[PF_6]), as well as the good match that we have observed between experimental data for **2**[PF_6] and **5**[PF_6] and theoretical predictions based on the simple two-level model initially developed by Hush[18] and subsequently implemented by others.[19–21]

Results

Synthesis and Characterization of the Heterodinuclear Complexes 2 and 5. The dinuclear compound **2** was obtained from reaction between the functional mononuclear Fe(II) alkynyl complex **6**,[22] containing a terminal ethyne functionality, and the five-coordinate [*cis*-Cl(dppe)$_2$Ru][OTf] (dppe = 1,2-bis-(diphenylphosphino)ethane) cation (**7**[OTf])[23] (Scheme 1). The analogue **5** was isolated from **2** after reaction with a 4-fold excess of *p*-nitrophenylacetylene under similar conditions. Both compounds were obtained in fair yields and were fully characterized by LSIMS, elemental analysis, cyclic voltammetry, and the usual spectroscopy (see the Experimental Section).

The ^{1}H and ^{31}P NMR spectra of **2** and **5** confirm the purity of the isolated samples and are diagnostic of iron- (near 100 ppm) and ruthenium-bound (50–55 ppm region) dppe ligands on acetylide metal centers;[24,25] as expected, these ^{31}P NMR signals are in a 1:2 ratio. One intense absorption is observed in the infrared spectra in the $\nu_{C\equiv C}$ region near 2055 cm^{-1}, characteristic of Ru(II) and Fe(II) acetylides. These broad absorptions correspond to the overlap of the two metal alkynyl stretches expected for the bridging ligand in **2** and **5**. These were previously reported at 2053 cm^{-1} for **8-H**,[24] at 2067 cm^{-1} for **9-H**,[25] and at 2052 cm^{-1} for **10** (Chart 2).[25] Notably, no additional metal alkynyl stretch is clearly detected for **5**, in spite of the presence of the 4-nitrophenylacetylide ligand on ruthenium, but a slight shoulder is apparent at ca. 2070 cm^{-1}. A corresponding feature appears as a very small peak at 2074 cm^{-1} for **10**.[26]

Synthesis and Characterization of the Heterodinuclear MV Complexes 2[PF_6] and 5[PF_6]. The MV complexes **2**[PF_6] and **5**[PF_6] were isolated from their neutral precursors by chemical oxidation using 1 equiv of ferrocenium hexafluorophosphate (Scheme 2). The large separation between the redox potentials corresponding to the mono- and dioxidized states ($\geq$0.65 V; see Table 1) permitted their clean isolation as red-brown solids.[3,4] The monooxidized compounds **2**[PF_6] and **5**[PF_6] exhibit the same cyclic voltammograms as their neutral parents, but infrared spectroscopy clearly reveals their oxidized nature. Thus, two $\nu_{C\equiv C}$ stretches are now observed for each of these compounds, one of them being located below 1950 cm^{-1},

(17) Olivier, C.; Choua, S.; Turek, P.; Touchard, D.; Rigaut, S. *Chem. Commun.* **2007**, 3100–3102.
(18) (a) Hush, N. S. *Prog. Inorg. Chem.* **1967**, *8*, 357–389. (b) Hush, N. S *Prog. Inorg. Chem.* **1967**, *8*, 391–444.
(19) Brunschwig, B. S.; Creutz, C.; Sutin, N. *Chem. Soc. Rev.* **2002**, *31*, 168–184.
(20) Nelsen, S. F. *Chem. Eur. J.* **2000**, *4*, 581–588.
(21) Demadis, K. D.; Hartshorn, C. M.; Meyer, T. J. *Chem. Rev.* **2001**, *101*, 2655–2685.
(22) Courmarcel, J.; Le Gland, G.; Toupet, L.; Paul, F.; Lapinte, C. *J. Organomet. Chem.* **2003**, *670*, 108–122.
(23) Polam, J. R.; Porter, L. C. *J. Coord. Chem.* **1993**, *29*, 109–119.
(24) Denis, R.; Toupet, L.; Paul, F.; Lapinte, C. *Organometallics* **2000**, *19*, 4240–4251.
(25) Touchard, D.; Haquette, P.; Guesmi, S.; Le Pichon, L.; Daridor, A.; Toupet, L.; Dixneuf, P. H. *Organometallics* **1997**, *16*, 3640–3648.
(26) Younus, M.; Long, N. J.; Raithby, P. R.; Lewis, J.; Page, N. A.; White, A. J. P.; Williams, D. J.; Colbert, M. C. B.; Hodge, A. J.; Khan, M. S.; Parker, D. G. *J. Organomet. Chem.* **1999**, *578*, 198–209.

Scheme 1. Synthesis of 2 and 5 ([Fe] = (η^2-dppe)(η^5-C_5Me_5)Fe and [Ru] = *trans*-(η^2-dppe)$_2$Ru)

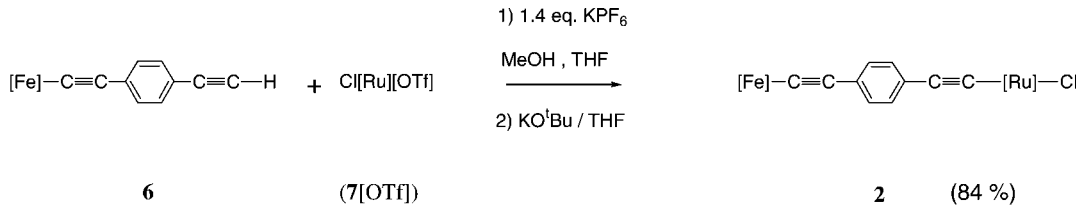

6 (**7**[OTf]) **2** (84 %)

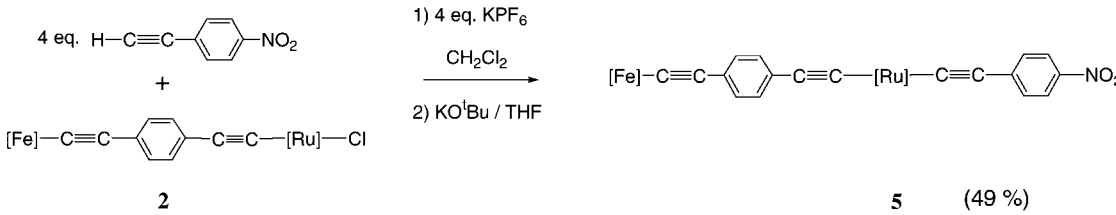

2 **5** (49 %)

Scheme 2. Synthesis of 2[PF_6] and 5[PF_6] ([Fe] = (η^2-dppe)(η^5-C_5Me_5)Fe and [Ru] = *trans*-(η^2-dppe)$_2$Ru)

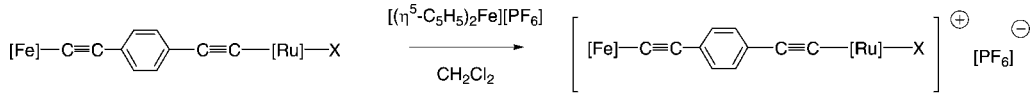

2 (X = Cl) **2**[PF_6] (X = Cl; 60 %)

5 (X = CC(4-$C_6H_4NO_2$)) **5**[PF_6] (X = CC(4-$C_6H_4NO_2$); 85 %)

Table 1. Electrochemical Data for Selected Complexes[a]

complex	E° (V)[b] Ru(III)/Ru(II)	Fe(III)/Fe(II)	$NO_2/NO_2^{\bullet-}$
[Fe]C≡C(C_6H_5) (**8-H**)		−0.15[c]/−0.14[c,e]	
Cl[Ru]C≡C(C_6H_5) (**9-H**)	0.44[d]/0.46[d,e]		
(C_6H_5)C≡C[Ru]C≡C (4-$C_6H_4NO_2$) (**10**)	0.55[d]		−1.25[d]
[Fe]C≡C(C_6H_4)C≡C [Ru]Cl (**2**)	0.41[d]	−0.24[d]	
[Fe]C≡C(C_6H_4)C≡C[Ru] C≡C(4-$C_6H_4NO_2$) (**5**)	0.50[d]	−0.23[d]	−1.25[d]

[a] [Fe] = (η^2-dppe)(η^5-C_5Me_5)Fe and [Ru] = *trans*-(η^2-dppe)$_2$Ru. [b] All E° values in V vs SCE. Conditions: CH_2Cl_2 solvent, 0.1 M (N^nBu_4)(PF_6) supporting electrolyte, 20 °C, Pt electrode, sweep rate 0.100 V s^{-1}. [c] The ferrocene/ferrocenium (Fc/Fc^+) couple was used as an internal reference for potential measurements. [d] The [Fe]C≡C(4-$C_6H_4NO_2$) complex was used as an internal reference for potential measurements.[27] [e] Measurement carried out in acetonitrile.

a region where Fe(III)[28] or Ru(III)[29,30] acetylide stretches typically appear.

The ESR spectra of these compounds in solvent glasses were then recorded along with the spectra of the monomeric compounds **8-H**[PF_6], **9-H**[BF_4], and **10**[BF_4], the latter being used as reference compounds. All of these radical cations were chemically generated in situ in CH_2Cl_2/1,2-$C_2H_4Cl_2$from their neutral parents at ambient temperature. Acetylferrocenium tetrafluoroborate was used to oxidize the monomeric complexes **9-H** and **10**, whereas ferrocenium hexafluorophosphate was used for the dinuclear complexes **2** and **5**.[31] Following the addition of the oxidant, the solutions were immediately frozen and the samples were kept at 80 K until the ESR measurements were completed. Similar ESR spectra were obtained from isolated samples of **2**[PF_6] and **5**[PF_6], obtained according to Scheme 2. In each case, rhombic signals exhibiting three *g* tensors were observed (Figure 1 and Table 2), in line with the presence of metal-centered radicals.[12,29] The presence of some ^{31}P hyperfine structure (ca. 13 G) is apparent on the g_3 tensor of **5**[PF_6] (Figure 1).[32] This feature is also observed, but less resolved, in the case of **2**[PF_6].

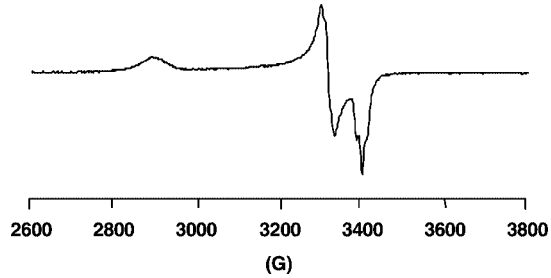

Figure 1. ESR spectrum of **5**[PF_6] in CH_2Cl_2/1,2-$C_2H_4Cl_2$ (1:1) at 80 K.

In the case of compounds **2** and **2**[PF_6], the Mössbauer spectra were also recorded at 80 K. Oxidation is accompanied by a decrease of the ^{57}Fe isomer shift from 0.26(1) to 0.25(2) mm s^{-1} and by a concomitant decrease of the quadrupolar splitting from 1.97(7) to 0.96(8) mm s^{-1}.

In order to further investigate the electronic structure of these MV complexes, a variable-temperature (VT) ^{1}H NMR study

(27) Costuas, K.; Paul, F.; Toupet, L.; Halet, J.-F.; Lapinte, C. *Organometallics* **2004**, *23*, 2053–2068.
(28) Paul, F.; Mevellec, J.-Y.; Lapinte, C. *Dalton Trans.* **2002**, 1783–1790.
(29) Paul, F.; Ellis, B. J.; Bruce, M. I.; Toupet, L.; Roisnel, T.; Costuas, K.; Halet, J.-F.; Lapinte, C. *Organometallics* **2006**, *25*, 649–665.
(30) Adams, C. J.; Pope, S. J. A. *Inorg. Chem.* **2004**, *43*, 3492–3499.
(31) Connelly, N. G.; Geiger, W. E. *Chem. Rev.* **1996**, *96*, 877–910.
(32) Connelly, N. G.; Gamasa, M. P.; Gimeno, J.; Lapinte, C.; Lastra, E.; Maher, J. P.; Le Narvor, N.; Rieger, A. L.; Rieger, P. H. *J. Chem. Soc., Dalton Trans.* **1993**, 2575–2578.

Table 2. ESR Data for Compounds in Frozen CH_2Cl_2/1,2-$C_2H_4Cl_2$ Solutions at 80 K[a]

complex	g_1[b]	g_2[b]	g_3[b]	Δg[b]	ref
[[Fe]C≡C(C_6H_5)][PF_6] (**8-H**[PF_6])	2.46(4)	2.03(3)	1.97(5)	0.48(9)	12
[Cl[Ru]C≡C(C_6H_5)][BF_4] (**9-H**[BF_4])	2.51(9)	2.03(9)	1.89(6)	0.62(3)	this work
[(C_6H_5)C≡C[Ru]C≡C(4-$C_6H_4NO_2$)][BF_4] (**10**[BF_4])	2.48(9)	2.03(6)	1.89(6)	0.59(3)	this work
[[Fe]C≡C(C_6H_4)C≡C[Ru]Cl][PF_6] (**2**[PF_6])	2.33(0)	2.03(9)	1.98(9)	0.34(1)	this work
[[Fe]C≡C(C_6H_4)C≡C[Ru]C≡C(4-$C_6H_4NO_2$)][PF_6] (**5**[PF_6])	2.33(7)	2.03(7)	1.98(8)[c]	0.34(9)	this work

[a] [Fe] = (η^2-dppe)(η^5-C_5Me_5)Fe and [Ru] = *trans*-(η^2-dppe)$_2$Ru. [b] The last digit is given in parentheses due to the experimental uncertainty of the measurements. [c] $A_{PRu} \approx 13.3$ G.

Table 3. UV–vis Data for Selected Complexes in CH_2Cl_2[a]

complex	abs (nm) ($10^{-3}\epsilon$ (M^{-1} cm^{-1}))	ref
[Fe]C≡C(C_6H_5) (**8-H**)	277 (sh, 14.5), 350 (13.6)	27
[[Fe]C≡C(C_6H_5)][PF_6] (**8-H**[PF_6])	261 (sh, 32.6), 280 (sh, 27.4), 301 (sh, 18.8), 342 (sh, 5.9), 379 (sh, 3.6), 575 (sh, 2.3), 662 (3.1)	12
Cl[Ru]C≡C(C_6H_5) (**9-H**)	319 (23.0)	10
(C_6H_5)C≡C[Ru]C≡C(4-$C_6H_4NO_2$) (**10**)	240 (63.1), 266 (sh, 32.7), 316 (22.9), 486 (21.2)	this work
[Fe]C≡C(C_6H_4)C≡C[Ru]Cl (**2**)	330 (sh, 24.0), 378 (32.3)	this work
[[Fe]C≡C(C_6H_4)C≡C[Ru]Cl][PF_6] (**2**[PF_6])	362 (23.5), 448 (sh, 12.1), 498 (15.1), 1124 (16.1)	this work
[Fe]C≡C(C_6H_4)C≡C[Ru]C≡C(4-$C_6H_4NO_2$) (**5**)	328 (26.7), 378 (32.3), 490 (22.0)	this work
[[Fe]C≡C(C_6H_4)C≡C[Ru]C≡C(4-$C_6H_4NO_2$)][PF_6] (**5**[PF_6])	354 (28.5), 464 (sh, 33.0), 493 (36.2), 1080 (18.3)	this work

[a] [Fe] = (η^2-dppe)(η^5-C_5Me_5)Fe and [Ru] = *trans*-(η^2-dppe)$_2$Ru.

Chart 2. Mononuclear Model Complexes Used throughout This Work

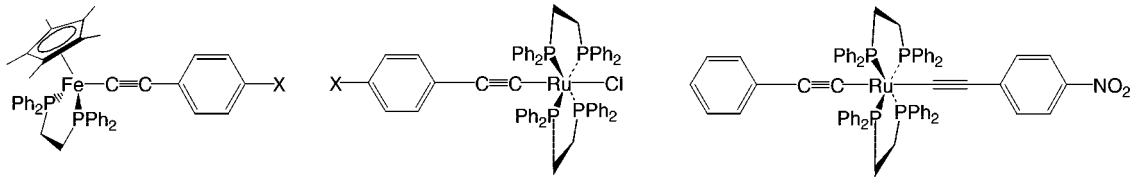

8-X **9-X** **10**

Scheme 3. Synthesis of 11 ([Ru] = *trans*-(η^2-dppe)$_2$Ru)

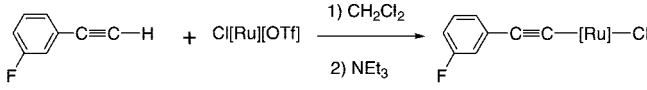

(**7**[OTf]) **11** (61 %)

was undertaken with **2**[PF_6]. All ^{1}H signals detected could be assigned by comparison with previous results obtained with the mononuclear model compounds **8-X**[PF_6].[33] Except for H_3 and H_4, which overlap with the dppe protons on ruthenium, the temperature-dependent shifts of the signals of the protons H_1−H_{11} correspond to those of previous observations (Figure 2); the dppe protons on ruthenium are only slightly affected by temperature. ^{31}P NMR spectra were also recorded for **2**[PF_6] in the +400 to −3500 ppm range. A broad signal ($\nu_{1/2}$ = 700 ± 100 Hz) is present in the diamagnetic region, above 100 ppm, but no additional signal could be detected at high field, where the dppe phosphorus atoms bound to Fe(III) are expected to appear.[33] The former signal is thus tentatively assigned to the four dppe phosphorus atoms bound to ruthenium. Very similar features were observed in the ^{1}H and ^{31}P NMR spectra of **5**[PF_6]. Notably, the protons belonging to the 4-nitrophenylacetylide ligand on ruthenium were not detected outside the diamagnetic region (0–10 ppm), consistent with a small spin density residing on the ruthenium center in this complex.

Electronic Spectroscopy of 2, 2[PF_6], 5, and 5[PF_6]. The electronic spectra of the MV complexes **2**[PF_6] and **5**[PF_6] were then investigated in the UV–vis−near-IR range and compared to those of their neutral parents **2** and **5**. The latter show a couple of strong absorptions in the visible range, centered at ca. 330 and 380 nm. In addition, **5** also exhibits an absorption at 490 nm (Table 3). These absorptions are responsible for the red-orange color of the neutral parents. After monooxidation, a new and strong absorption appears in the near-IR range near 1100 nm for both **2**[PF_6] and **5**[PF_6], and the absorptions previously observed near 330 and 380 nm are now red-shifted by ca. 120 nm and weakened in intensity. As a result, the oxidized complexes are red-brown. It is noteworthy that the low-energy absorption of the nitro complex **5** at 490 nm is apparently not significantly affected by oxidation.

Given the possibility that we would observe an intervalence charge-transfer (IVCT) transition with these dinuclear MV complexes, particular attention was paid to the low-energy absorptions detected for **2**[PF_6] and **5**[PF_6]. These absorptions are very intense and exhibit a composite line shape, with the occurrence of several underlying processes (Figure 3a). An overall negative solvatochromism ($\Delta\bar{\nu} \approx 900$ cm^{-1}) is evident for this absorption in **2**[PF_6], the most intense contribution being clearly blue-shifted in more polar solvents (Figure 4). Regardless of the solvent used, the near-IR absorption of **2**[PF_6] can be deconvoluted into three Gaussian-shaped contributions, two of which (II and III) at higher energies are always separated by ca. 2200 cm^{-1} and appear much more solvent-sensitive than the third one (I) near 5900 cm^{-1} (Table 4). Similar to the case for **2**[PF_6], the intense near-IR absorption of **5**[PF_6] can be deconvoluted into three Gaussian contributions resembling those observed for **2**[PF_6] (Figure 3b and Table 4).

Synthesis and Characterization of Cl(η^2-dppe)$_2$Ru[C≡C(3-C_6H_4F)] (11). The new mononuclear complex Cl(η^2-dppe)$_2$Ru[C≡C(3-C_6H_4F)] (**11**) was needed in order to determine the electronic substituent parameter (ESP) of the "−(C≡C)-

(33) Paul, F.; da Costa, G.; Bondon, A.; Gauthier, N.; Sinbandhit, S.; Toupet, L.; Costuas, K.; Halet, J.-F.; Lapinte, C. *Organometallics* **2007**, *26*, 874–896.

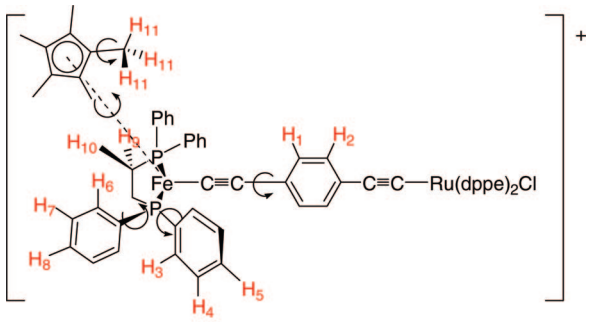

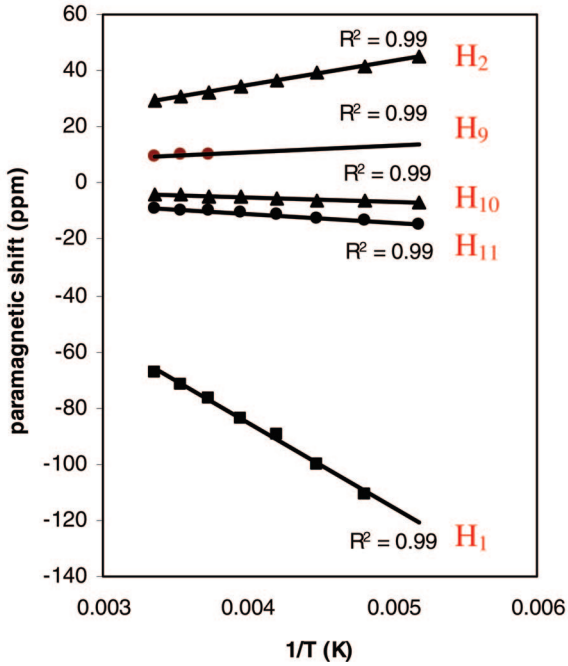

Figure 2. Temperature dependence of the ^{1}H NMR shifts of **2**[PF_6] in CD_2Cl_2 with proposed assignment for selected protons.

Ru(η^2-dppe)$_2$Cl" organoruthenium fragment by ^{19}F NMR (see below). This complex was thus synthesized from the triflate precursor complex **7**[OTf] (Scheme 3), following an original synthesis inspired from that used to obtain **2**. The desired complex was isolated in fair yields and fully characterized by the usual means (see the Experimental Section).

Yellow crystals of **11**·$2CH_2Cl_2$ could be grown by slow evaporation of the solvent from a dichloromethane solution of the complex. The solid-state structure obtained by X-ray

Scheme 4. The Two Redox Isomers of the MV Complexes 2^+ (X = Cl) and 5^+ (X = C≡C(4-$C_6H_4NO_2$)) in the GS

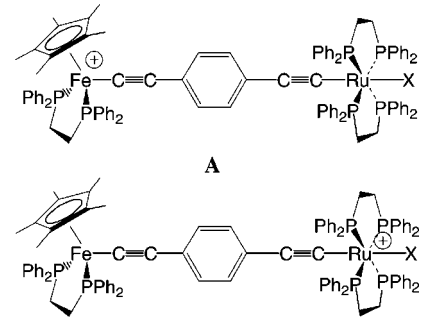

Chart 3. Mononuclear Model Complexes Used to Derive the ESPs of the Organoruthenium Substituent

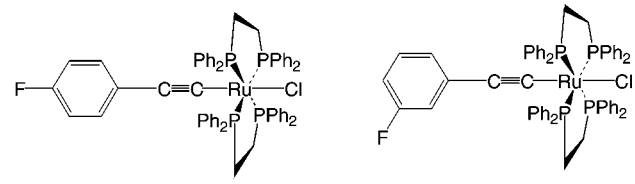

diffractometry confirms the structure of complex **11** (Figure 5). The complex crystallizes in the monoclinic $P2_1/n$ space group with one molecule of complex in the asymmetric unit and two dichloromethane solvates (see the Experimental Section for details). The bond lengths and angles of this complex are unexceptional, in comparison with available X-ray data on related mononuclear Ru(II) acetylide complexes,[26,34] apart from the rather short length of the C≡C triple bond (ca. 1.10 Å). The latter feature might, however, be an artifact resulting from the poor quality of the diffraction data set (R_{int} = 0.0869).

Discussion

Electronic Structure of the Ground State (GS) of the MV Complexes 2[PF_6] and 5[PF_6]. While the rhombic ESR spectra obtained for **2**[PF_6] and **5**[PF_6] at 80 K evidence the metal-centered nature of the unpaired electron in these compounds, unambiguous assignment of the location of the unpaired electron is not possible from these data alone, since very similar rhombic spectra were obtained for the mononuclear iron(III) (**8-H**[PF_6]) and ruthenium(III) (**9-H**[BF_4], **10**[BF_4]) complexes used as references (Table 2). However, the slight change in anisotropy (Δg) between **2**[PF_6] and **5**[PF_6] reveals that the

Table 4. Near-IR Data for 2[PF_6] and 5[PF_6] in Dichloromethane and Acetonitrile[a]

[Fe$^+$]C≡C(C_6H_4)C≡C[Ru]X	band	$\bar{\nu}_{max}$ (cm^{-1})[b] (ϵ (M^{-1} cm^{-1}))[c]	$(\Delta\bar{\nu}_{1/2})_{exptl}$ (cm^{-1})	$\Delta G°$ (cm^{-1})	$(\Delta\bar{\nu}_{1/2})_{theor}$ (cm^{-1})[c,d]	H_{ab} (cm^{-1})[b]
X = Cl (**2**$^+$)	I	5900 (1750)	1500	4760	1620	
		5950 (1100)[e]	1500[e]	4840[e]	1600	
	II	8900 (16100)	2670	4760	3090	1060[f]/2070[g]
		9500 (12600)[e]	2830[e]	4840[e]	3280	1000[e,f]/2330[e,g]
	III	11100 (1100)	2670	4760	3830	
		11750 (1700)[e]	2830[e]	4840[e]	4000	
X = C≡C(C_6H_4)NO_2 (**5**$^+$)	I	5900 (1200)	1500	5650	760	
	II	9230 (18100)	2660	5650	2880	1150[f]/1790[g]
	III	11800 (1150)	2750	5650	3770	

[a] [Fe] = (η^2-dppe)(η^5-C_5Me_5)Fe and [Ru] = *trans*-(η^2-dppe)$_2$Ru. [b] Values ±50 cm^{-1}. [c] Values ±5%. [d] Calculated following eq 1. Note that these values are only appropriate for IVCT bands; they are included here to illustrate the incompatibility between the experimental half-widths measured for some bands and those calculated from the classical Hush model. [e] Values found in CH_3CN. [f] Calculated following eq 2 with d_{ab} = 12 Å. [g] Calculated for a class III MV complex ([ν_{max} − $\Delta G°$]/2).

unpaired electron is only slightly affected by the change in the apical ligand on ruthenium, suggesting at most a weak delocalization to this metal center.[35]

Stronger indications about the localization of the electronic hole/unpaired electron in these MV complexes can be gathered from CV data. The first oxidation potentials of **2** and **5** at −0.24 and −0.23 V, respectively, vs the saturated calomel electrode (SCE) are more cathodic than that observed for the mononuclear iron model complex **8-H** (−0.15 V vs SCE)[24] but are even more cathodic than those of the corresponding mononuclear ruthenium models **9-H**[10,26,34] (0.44 vs SCE) and **10**[26] (0.55 vs SCE). Thus, the oxidation likely corresponds to an iron-centered process in **2** and **5**.

Firmer evidence for the dominant localization of the electronic vacancy on iron in **2**[PF_6] or **5**[PF_6] comes from the NMR and Mössbauer investigations performed on **2**[PF_6]. First, the ^{1}H NMR spectrum of **2**[PF_6] is diagnostic of an iron-centered radical. Thus, the proton signals are significantly shifted compared to their corresponding values in the diamagnetic parent **2** when located in the coordination sphere of iron, whereas they stay very close to their position in the spectrum of the diamagnetic complex **9-H** when located in the coordination sphere of ruthenium, in line with a negligible spin delocalization to this metal center.[33] In addition, the quadrupolar separation (ΔQ) value of 0.97 ± 0.01 of the ^{57}Fe Mössbauer doublet for **2**[PF_6] is also diagnostic of a Fe(III) center in the solid state.[36] Thus, the electronic structure of **2**[PF_6] or **5**[PF_6] in the GS might be more accurately described by the valence bond (VB) isomer A instead of B (Scheme 4).

On the basis of Hammett correlations previously established,[27] **2** or **5** can be considered as mononuclear compounds such as **8-X**, in which a strongly electron-releasing organometallic substituent is appended to the arylacetylide ligand in place of X. From the linear free energy relationships (LFERs) involving the first oxidation potentials, Hammett σ_p electronic substituent parameters (ESPs) of −0.54 ± 0.06 and of −0.48 ± 0.06 would be obtained for the "−(C≡C)Ru(η^2-dppe)$_2$Cl" and "−(C≡C)-Ru(η^2-dppe)$_2$[C≡C(4-$C_6H_4NO_2$)]" substituents, respectively. The first of these values is, however, significantly larger than the σ_p value of −0.34 ± 0.04, which can be derived independently for the "−(C≡C)Ru(η^2-dppe)$_2$Cl" organoruthenium fragment by ^{19}F NMR from the *p*- (**9-F**) and *m*-fluoro derivatives (**11**; Chart 3), according to the method originally proposed by Taft and co-workers.[37] This latter value actually suggests that the "−(C≡C)Ru(η^2-dppe)$_2$Cl" substituent should be slightly more electron-releasing than a methoxy group in **2**; this statement is also supported by the anisotropy of the ESR spectrum of **2**[PF_6], on the basis of correlations between the anisotropy and the σ^+ ESPs previously established for **8-X**[PF_6] radicals and considering that the electronic vacancy in **2**[PF_6] is mostly located on iron (Scheme 4).[12]

Thus, at least for **2**, and solely on the basis of $E°$ values, it seems that the electron-releasing capability of the organoruthenium unit is slightly overestimated in the LFERs established for the model complexes **8-X**. Conversely, this also means that the $E°$ value corresponding to the Fe(II)/Fe(III) oxidation is too large to result solely from inductive/mesomeric substituent effects. We will come back to this statement later on. Note also that the potential separation $\Delta E°$ between the two

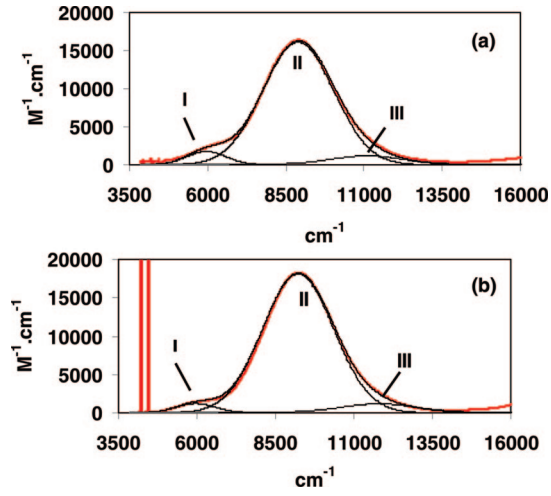

Figure 3. Deconvolution of the broad near-IR absorption (a) at 1124 nm for **2**[PF_6] and (b) at 1080 nm for **5**[PF_6] in CH_2Cl_2.

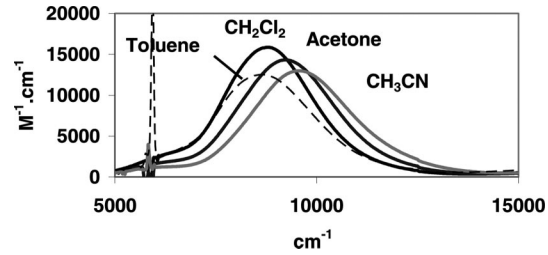

Figure 4. Solvatochromic behavior of the broad near-IR absorption for **2**[PF_6]. The absorption recorded in THF has been omitted for clarity.

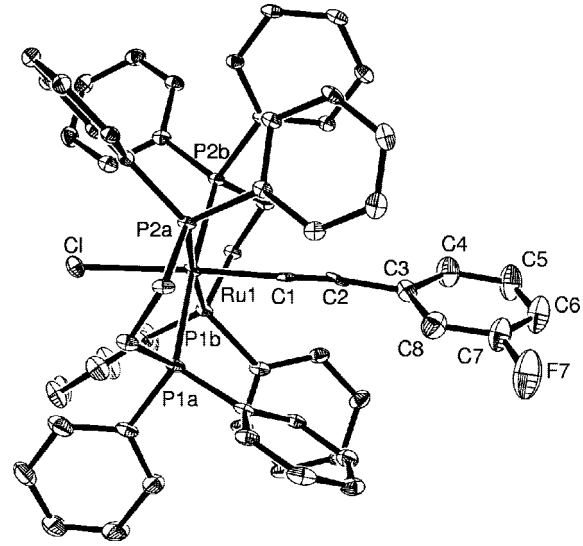

Figure 5. ORTEP plot of **11**. Thermal ellipsoids are at the 30% probability level. Hydrogen atoms have been omitted for clarity.

(34) (a) Hurst, S. K.; Cifuentes, M. P.; Morrall, J. P. L.; Lucas, N. T.; Whittall, I. R.; Humphrey, M. G.; Asselberghs, I.; Persoons, A.; Samoc, M.; Luther-Davies, B.; Willis, A. C. *Organometallics* **2001**, *20*, 4664–4675. (b) Morrall, J. P.; Cifuentes, M. P.; Humphrey, M. G.; Kellens, R.; Robijns, E.; Asselberghs, I.; Clays, K.; Persoons, A.; Samoc, M.; Willis, A. C. *Inorg. Chim. Acta* **2006**, *359*, 998–1005.

(35) In line with that statement, the poorly resolved ^{31}P hyperfine structure apparent on the g_3 tensor in the ESR spectrum of **5**[PF_6] (Figure 1) is more reminiscent of a triplet than of a quintet, suggesting that the unpaired electron mostly sees two phosphorus atoms rather than four, in accordance with its dominant localization on the iron center.

(36) Argouarch, G.; Thominot, P.; Paul, F.; Toupet, L.; Lapinte, C. *C. R. Chim.* **2003**, *6*, 209–222.

(37) (a) Taft, R. W.; Price, E.; Fox, I. R.; Lewis, I. C.; Andersen, K. K.; Davies, G. T. *J. Am. Chem. Soc.* **1963**, *85*, 3146–3156. (b) Taft, R. W.; Price, E.; Fox, I. R.; Lewis, I. C.; Andersen, K. K.; Davies, G. T. *J. Am. Chem. Soc.* **1963**, *85*, 709–724.

reversible redox potentials corresponding to the metal-centered oxidations in this compound (0.65 V) is quite close to the difference between the redox potentials of the corresponding oxidations in the monomer model complexes **8-H** and **9-H** (0.59 V), consistent with the redox centers in **2**[PF_6] not being so strongly coupled that it renders the Hush model inapplicable.

Electronic Delocalization in MV Complexes 2[PF_6] and 5[PF_6]. On the basis of the data available for **8-H**, **9-H**, and **10** (Table 3), the low-energy absorptions observed in the range 330–500 nm most likely correspond to MLCT transitions for **2** and **5**.[10,26,27,34] More specifically, by comparison with the low-energy transition observed for **10** at 486 nm (Table 3), the low-energy transition of **5** observed at 493 nm is proposed to correspond to a $d_{Ru} \rightarrow (\pi^*)_{ArNO_2}$ excitation. Consistent with the localization of the unpaired electron being predominantly on iron (Scheme 4), this electronic transition does not seem to be strongly affected by oxidation. According to previous work with the mononuclear Fe(III) complexes **8-X**[PF_6], the LMCT transitions $\pi_{Ar} \rightarrow d_{Fe}$ are expected to arise in the same energy range for **2**[PF_6] and **5**[PF_6].[12]

The appearance of an intense absorption in the near-IR range for both MV complexes is more puzzling. On the basis of the data available for the corresponding symmetric MV complexes **1**[PF_6] and **3**[PF_6][4,13] and of the $\Delta G°$ gap deduced from the first oxidation potentials of the model complexes **8-H** and **9-H** by cyclic voltammetry (4760 cm^{-1}),[38] an IVCT is expected in this spectral region on the basis of the Hush model.[39] Indeed, considering the $\lambda_{Fe} \approx 4000$ cm^{-1} and $\lambda_{Ru} \approx 6500$ cm^{-1} values previously reported for the reorganization energies of **1**[PF_6][4] and **3**[PF_6],[13] respectively, the IVCT band should be found at around 10 000 cm^{-1} for **2**[PF_6]. This value is reasonably close to the intense absorption detected for this compound at ca. 8890 cm^{-1} (1124 nm). In addition, the negative solvatochromism exhibited by this absorption (Figure 4) would also be consistent with an IVCT transition of a weakly coupled MV complex. However, since this absorption exhibits a composite shape (Figure 3a), the various underlying contributions must now be identified in order to further support our hypothesis.

The contribution at lowest energy (I) probably corresponds to a d−d ligand field (LF) transition. Such transitions are usually observed with related Fe(III) complexes.[4,12] The weak solvatochromism of this contribution established with **2**[PF_6], as well as its spectral characteristics in **2**[PF_6] and **5**[PF_6], is consistent with this attribution.

Additional insight about the nature of the two remaining contributions is available by comparing the deconvolutions obtained for **2**[PF_6] and **5**[PF_6] (Table 4). Thus, replacement of the apical chloride atom by a less π-donating ligand such as the 4-nitrophenylacetylide should have a sizable influence on any transition involving the Ru(II) center, such as an IVCT transition, but should affect to a much lesser extent any transition involving the bridging ligand, such as an LC or LMCT transition. In accord with our hypothesis, the band I at lowest energy is shifted very slightly on proceeding from **2**[PF_6] to **5**[PF_6], as might be expected for a LF transition centered on the Fe(III) terminus. As is the case with **2**[PF_6], contributions II and III are separated by ca. 2500 cm^{-1} in **5**[PF_6] but are now shifted toward higher energies by ca. 350 cm^{-1}, as would be expected for IVCT transitions when the Ru(II) center is rendered more electron-poor. This observation, along with the fact that both transitions have the same half-widths, suggests that contributions II and III are associated with similar types of electronic transitions in **2**[PF_6] and **5**[PF_6] and confirms that they involve the ruthenium center to some extent, in line with their purported IVCT nature.

Note that low-energy transitions in the 600–900 nm range have also been observed for the Fe(III) model complexes **8-X**[PF_6], featuring electron-releasing substituents.[12] Such absorptions were observed at 718 nm for the methoxy-substituted complex (X = OMe) and at 894 nm for the dimethylamino substituent (X = NMe_2) and have been previously attributed to LMCT transitions. A closer inspection reveals, however, that the most intense contribution (i.e., band II) in both **2**[PF_6] and **5**[PF_6] is significantly more intense and broader than the low-energy transitions previously observed for **8-X**[PF_6] ($\bar{\nu}_{1/2} < 1800$ cm^{-1} for X = OMe and $\bar{\nu}_{1/2} < 2400$ cm^{-1} for X = NMe_2). In addition, the solvatochromic behavior of contributions II and III for **2**[PF_6] is markedly more pronounced than that of the low-energy bands of **8-OMe**[PF_6] ($\Delta\bar{\nu} \approx 200$ cm^{-1}) or **8-NMe_2**[PF_6] ($\Delta\bar{\nu} \approx 370$ cm^{-1}), which can be rationalized by the enhanced charge transfer taking place in **2**[PF_6] and **5**[PF_6]. All these observations strongly suggest that the nature of the near-IR transitions observed for the heterodinuclear MV complexes **2**[PF_6] and **5**[PF_6] might be somewhat different from those corresponding to the low-energy transitions previously observed with **8-X**[PF_6].

$$(\Delta\bar{\nu}_{1/2})_{theor} = [2310(\bar{\nu}_{max} - \Delta G°)]^{1/2} \quad (1)$$

$$H_{ab} = (2.06 \times 10^{-2}/d_{ab})(\epsilon_{max}\bar{\nu}_{max}\Delta\bar{\nu}_{1/2})^{1/2} \quad (2)$$

According to the Hush model applied to class-II unsymmetrical MV complexes (eq 1), the theoretical bandwidth of an IVCT transition is related to $\Delta G°$, the energy gap between the two potential wells corresponding to the two diabatic redox states A and B (Scheme 4) on the reaction coordinate axis, and to $\bar{\nu}_{max}$, the energy of the peak maximum.[2,5] For **2**[PF_6], this quantity ($\Delta G°$) was estimated from the difference in the oxidation potentials of the monomeric model complexes **8-H** and **9-H** in dichloromethane and amounts to ca. 4760 cm^{-1} (see above). As shown in Table 4, the theoretical half-width $(\Delta\bar{\nu}_{1/2})_{theor}$ of the IVCT computed according to eq 1 is close to that found experimentally for curve II [$(\bar{\nu}_{1/2})_{exptl}^{II}$] and also corresponds well with the $(\bar{\nu}_{1/2})_{exptl}$ value measured experimentally for the whole near-IR absorption of **2**[PF_6] (Table 4). This brings further credence to its assignment as an IVCT transition. Another experimental observation that supports such an assignment is the fact that band II becomes broader and is also shifted to higher energy in more polar solvents, a trend in line with predictions of eqs 1 and 3.[2,39] In contrast, the third contribution (III) is too narrow to correspond to another IVCT transition in the GS but could likely correspond to an IVCT transition involving an excited state of **2**[PF_6], as observed previously with **1**[PF_6].[2,40] Such transitions often result when low-lying LF states are present.

Assuming that band II corresponds to an IVCT transition, the electronic coupling (H_{ab}) of the MV complexes **2**[PF_6] and **5**[PF_6] amounts to 1060 ± 50 and 1150 ± 50 cm^{-1} (Table 1), respectively, according to eq 2, when the Fe−Ru (d_{ab}) distances

(38) $\Delta G° = e[E°_{\mathbf{9\text{-}H}} - E°_{\mathbf{8\text{-}H}}]$ (in this expression, *e* represents the charge of the electron).

(39) Creutz, C. *Prog. Inorg. Chem.* **1983**, *30*, 1–73.

(40) Note that this weak contribution (III) is required by the slight asymmetry of the band shape of the near-IR absorption. It could also be an artifact resulting from an unresolved vibronic progression. See for instance: Bailey, S. E.; Zink, J. I.; Nelsen, S. F *J. Am. Chem. Soc.* **2003**, *125*, 5939–5947.

are taken as 12 Å.[41] Despite the sizable uncertainties associated with the spectroscopic measurements and the sensitivity of the compounds, these values provide support for the proposition that quite similar electronic couplings are operative in **2**[PF_6] and **5**[PF_6].

The solvent has only a minor influence on the magnitude of the electronic coupling (H_{ab}) in **2**[PF_6]. Thus, proceeding from dichloromethane to acetonitrile does not significantly affect the stability of the MV complex **2**[PF_6], as evidenced by the similar $\Delta E°$ values found (Table 2), nor does it modify the electronic coupling (see Table 4).

When the entropy associated with the solvent reorganization is neglected, an estimate of λ can then be derived for these heterodinuclear MV compounds using eq 3 and $\Delta G°$ (Table 4). For both compounds the reorganization energy is larger than twice the electronic coupling ($2H_{ab} < \lambda$); thus, these compounds can be considered as class II MV complexes in the classification of Robin and Day,[42] as is also suggested from electrochemical data and from the negative solvatochromic behavior exhibited by the IVCT transition of **2**[PF_6].[2] Considering that $2H_{ab}/\lambda > [1 - (\Delta\bar{\nu}_{1/2})_{theor}/2\lambda]$, they can be further categorized as class IIA MV compounds according to the subcategorization developed for symmetric MV complexes by Brunschwig et al.[19] However, because the sizable electronic coupling of these MV complexes is certainly somewhat underestimated by the Hush treatment, they might be close to borderline class IIA/class IIB MV complexes. In other words, they are strongly coupled MV complexes with a "localized" valency on the NMR time scale in the GS.[21]

While the strong intensity of the bands II and III can appear surprising for IVCTs in localized MV complexes such as **2**[PF_6] and **5**[PF_6], it is quite likely that the strong electronic coupling and the less stringent symmetry restrictions operative for these nonsymmetric compounds are responsible for the strong intensity and asymmetric shape of the bands. In these unsymmetrical MV complexes, charge transfer occurs in the same direction for the LMCT and the IVCT transitions, and symmetry rules do not forbid the mixing of these transitions; the present data are thus consistent with the low-energy "LMCT" transitions previously observed in mononuclear Fe(III) complexes **8-X**[PF_6] acquiring an increasing "substituent" character as X becomes more and more able to accommodate an electronic vacancy, eventually transforming into IVCT transitions for the heterodinuclear MV compounds **2**[PF_6] and **5**[PF_6].

$$\bar{\nu}_{max} \approx \lambda + \Delta G° \quad (3)$$

$$\Delta G_{deloc} \approx (H_{ab})^2/(\lambda + \Delta G°) \approx (H_{ab})^2/\bar{\nu}_{max} \quad (4)$$

Using eq 4[5,39] and the available data to derive an estimate of the contribution of the electronic coupling to the separation between the redox waves ($\Delta E_{deloc} = \Delta G_{deloc}/e$), we find values of ca. 0.015 V for **2**[PF_6] and 0.018 V for **5**[PF_6]. Despite the experimental uncertainties associated with the redox potentials under our conditions (±0.01 V), it is clear that the electronic coupling contributes a significant part of the small increase in the separation between the first and second oxidation potentials in the dinuclear complexes, relative to those of the mononuclear

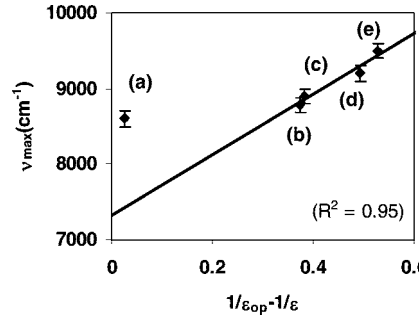

Figure 6. Solvent dependence of the near-IR band maximum (ν_{max}) for **2**[PF_6]: (a) toluene (not included in the correlation coefficient); (b) thf; (c) dichloromethane; (d) acetone; (e) acetonitrile.

model compounds,[43] the rest of the difference being attributable to synergistic, statistical, and magnetic contributions.[44]

$$\lambda_{out} = (\Delta e)^2[(1/2a_{Fe}) + (1/2a_{Ru}) - (1/d_{ab})](1/D_{op} - 1/D_s) \quad (5)$$

Finally, we have also plotted ν_{max} against the solvent function (Figure 6). If the point corresponding to toluene is not considered,[45] a linear relationship is found for the most polar solvents, in accordance with the Hush model (eqs 3 and 4). According to eq 5, the intercept at 7310 cm^{-1} corresponds to $\lambda_{in} + \Delta G°$, which permits us to obtain an approximate value for the internal contribution to the reorganization energy $\lambda_{in} =$ 2550 cm^{-1}. This estimate seems somewhat high for the internal reorganization energy according to theoretical and experimental estimates available in the literature for purely "inorganic" MV complexes.[39] However, it is well-known that such extrapolations often overestimate the true value of λ_{in}. Alternatively, the high value presently found might also reflect the large "organic" character of the "ruthenium-centered" excited-state of **2**[PF_6]. In comparison, $\lambda_{out} = 1590$ cm^{-1} constitutes a smaller component of the reorganization energy involved during the electron transfer in **2**[PF_6].

Conclusion

We have shown in this contribution that the intense absorptions present in the near-IR region (near 1100 nm) of electronic spectra of unsymmetrical MV complexes such as **2**[PF_6] and **5**[PF_6] likely correspond to IVCT transitions. In contrast to related symmetrical dinuclear MV compounds featuring only electron-rich organoruthenium end groups such as **3**[PF_6], the spectral features of these bands in the unsymmetrical complexes investigated herein obey predictions based on the Hush model. This behavior might be ascribed to the presence of the electron-rich iron end group "(η^2-dppe)(η^5-C_5Me_5)Fe", which tends to localize the electronic vacancy on the iron in the GS. On the basis of the assumption that the near-IR transition corresponds to an IVCT transition, an effective electronic coupling of ca. 1100 cm^{-1} can be derived between this end group and the second Ru-based redox-active end group "−(C≡C)Ru(η^2-dppe)$_2$(X)" (X = Cl, C≡C(4-$C_6H_4NO_2$)) in both **2**[PF_6] and

(41) In eq 3, ϵ_{max}, $\bar{\nu}_{max}$ and $\Delta\bar{\nu}_{1/2}$ are the extinction coefficient, the energy of the maximum, and the half-width of the IVCT band, respectively. The Fe−Ru (d_{ab}) distance was estimated from DFT modeling and from X-ray data on related complexes.

(42) Robin, M. B.; Day, P. *Adv. Inorg. Chem. Radiochem.* **1967**, *10*, 247–422.

(43) $\Delta E°_1 - [E°_{6\text{-}H} - E°_{8\text{-}H}] = 0.06$ V and $\Delta E°_5 - [E°_{11} - E°_{8\text{-}H}] = 0.03$ V.

(44) Evans, C. E. B.; Naklicki, M. L.; Rezvani, A. L.; White, C. A.; Kondratiev, V. V.; Crutchley, R. J. *J. Am. Chem. Soc.* **1998**, *120*, 13096–13103.

(45) We have presently no explanation for this discrepancy, but specific solute−solute or solute−solvent interactions might be at the origin of the "higher-than-expected" $\bar{\nu}_{max}$ value found.

5[PF_6]. This value would unambiguously categorize these open-shell species as sizably coupled class II MV complexes in the classification of Robin and Day.

Experimental Section

General Data. All manipulations were carried out under an inert atmosphere. Solvents and reagents were used as follows: Et_2O and *n*-pentane, distilled from Na/benzophenone; CH_2Cl_2, distilled from CaH_2 and purged with Ar, opened/stored under Ar. The [(η^5-$C_5H_5)_2$Fe][PF_6] ferrocenium salt was prepared by previously published procedures.[31] High-field NMR spectra experiments were performed on a multinuclear Bruker 500, 300, or 200 MHz instrument (AVANCE 500, AM300WB, and 200DPX). Chemical shifts are given in parts per million relative to tetramethylsilane (TMS) for ^{1}H and ^{13}C NMR spectra, external H_3PO_4 for ^{31}P NMR spectra, and external fluorotrichloromethane for ^{19}F NMR spectra. Transmittance-FTIR spectra were recorded using a Bruker IFS28 spectrometer (400–4000 cm^{-1}). Near-IR and UV–visible spectra were recorded using a Cary 5000 spectrometer. ESR spectra were recorded on a Bruker EMX-8/2.7 (X-band) spectrometer. The Mössbauer spectra were recorded with a 2.5×10^{-2} C (9.25×10^8 Bq) ^{57}Co source using a symmetric triangular sweep mode.[46] MS analyses were performed at the "Centre Regional de Mesures Physiques de l'Ouest" (CRMPO, University of Rennes) on a high-resolution MS/MS ZABSpec TOF Micromass spectrometer. Elemental analyses were performed at the "Centre Regional de Mesures Physiques de l'Ouest" (CRMPO, University of Rennes). The solid-state structure (X-ray) was resolved at the "Centre de Diffractométrie X" (UMR CNRS 6226, University of Rennes).

Unless specified, all reagents were of commercial grade. The complexes **6**,[22] **7**,[23] **9-H**,[25] **9-F**[34b] and **10**[25] were obtained according to reported syntheses.

Synthesis of (η^2-dppe)(η^5-C_5Me_5)Fe[C≡C-1,4-(C_6H_4)C≡C]-Ru(η^2-dppe)$_2$Cl (2). In a Schlenk tube, [RuCl(dppe)$_2$][OTf] (**7**; 0.242 g, 0.224 mmol) and KPF_6 (0.058 g, 0.315 mmol) were dissolved in 20 mL of THF. The complex (η^2-dppe)(η^5-C_5Me_5)Fe[C≡C(4-C_6H_4C≡CH)] (**6**; 0.160 g, 0.224 mmol) was then slowly added before addition of 50 mL of methanol. The solution was stirred for 2 days at room temperature, and the solvent was removed in vacuo. The remaining residue was extracted with dichloromethane and the extract concentrated in vacuo. Several washings with diethyl ether yielded a slightly air-sensitive brown solid. This solid was stirred for 4 h in THF in the presence of excess of KO^{t}Bu (0.041 g, 0.362 mmol). After removal of the solvent, extraction with toluene, concentration of the extract to dryness, and subsequent washing with *n*-pentane, the desired red complex **2** was isolated (0.250 g, 0.152 mmol; 84%). Anal. Calcd for $C_{98}H_{91}ClFeP_6Ru$: C, 71.47; H, 5.57. Found: C, 71.43; H, 5.56. MS (ESI): *m*/*z* 1646.3652 ($M^{\bullet+}$), calcd for $C_{98}H_{91}ClFeP_6Ru$ 1646.3628 ($M^{\bullet+}$). FT-IR (ν, KBr, cm^{-1}): 2056 (FeC≡C and RuC≡C). ^{31}P NMR (81 MHz, C_6D_6, δ in ppm): 101.7 (s, 2P, (dppe)Fe), 50.9 (s, 4P, (dppe)$_2$Ru). ^{1}H NMR (300 MHz, CD_2Cl_2, δ in ppm): 7.97 (m, 4H, $H_{Ar/dppe}$), 7.44–6.99 (m, 56H, $H_{Ar/dppe}$), 6.75 (d, 2H, $^3J_{HH}$ = 8.2 Hz, H_{Ar}), 6.50 (d, 2H, $^3J_{HH}$ = 8.2 Hz, H_{Ar}), 2.74 (m, 10H, CH_2), 2.10 (m, 2H, CH_2), 1.49 (s, 15H, $C_5(CH_3)_5$). ^{13}C{^{1}H} NMR (75 MHz, CD_2Cl_2, δ in ppm): 140.3–125.3 ($C_{Ar/dppe}$ + Fe*C*≡C + Ru*C*≡C), 126.3 (s, C_{Ar}), 125.0 (s, C_{Ar}), 120.0 (s, FeC≡*C*), 114.0 (s, RuC≡*C*), 87.7 (s, $C_5(CH_3)_5$), 30.9 (m, $(CH_2)_{dppe/Ru\&Fe}$), 10.2 (s, $C_5(CH_3)_5$). CV (CH_2Cl_2, 0.1 M *n*-$Bu_4N^+PF_6^-$, 20 °C, 0.1 V s^{-1}; $E°$ in V vs SCE (ΔE_p in V, $i_{p,a}/i_{p,c}$)): −0.24 (0.08, 1.0), 0.41 (0.08, 1.0). Mössbauer (mm s^{-1} vs ^{57}Fe, 80 K): IS 0.26(1), QS 1.97(7).

Synthesis of [(η^2-dppe)(η^5-C_5Me_5)Fe[C≡C-1,4-(C_6H_4)C≡C]-Ru(η^2-dppe)$_2$Cl][PF_6] (2[PF_6]). [(η^5-$C_5H_5)_2$Fe][PF_6] (0.040 g, 0.121 mmol) was added to a solution of **2** (0.210 g, 0.128 mmol) in dichloromethane. Stirring was maintained for 1.5 h at 20 °C, and the solution was concentrated in vacuo. Addition of diethyl ether resulted in the precipitation of **2**[PF_6], which could be isolated (0.138 g, 0.077 mmol, 60%) after subsequent washings with toluene (5 mL), diethyl ether (10 mL), and *n*-pentane (10 mL). FT-IR (ν, KBr/CH_2Cl_2, cm^{-1}): 2034/2038 (m, RuC≡C), 1943/1947 (s, FeC≡C). ^{31}P NMR (81 MHz, $CDCl_3$, δ in ppm): 103.3 (broad s, P, Ru(dppe)$_2$). ^{1}H NMR (500 MHz, CD_2Cl_2, δ in ppm, numbering according to Figure 2): 29.1 (s, 2H, H_2), 9.6 (broad s, 2H, H_9), 8.1–6.8 (m, 52H, $H_{Ar/dppe}$), 4.4 (s, 4H, H_6 or H_7), 4.2 (s, 4H, H_6 or H_7), 2.6 (s, 8H, $(CH_2)_{dppe/Ru}$), −4.0 (s, 2H, H_{10}), −9.0 (s, 15H, H_{11}), −66.8 (s, 2H, H_1). Mössbauer (mm s^{-1} vs ^{57}Fe, 80 K): IS 0.25(2), QS 0.96(8).

Synthesis of (η^2-dppe)(η^5-C_5Me_5)Fe[C≡C-1,4-(C_6H_4)C≡C]-Ru(η^2-dppe)$_2$[C≡C(4-$C_6H_4NO_2$)] (5). In a Schlenk tube, (η^2-dppe)(η^5-C_5Me_5)Fe[C≡C-1,4-(C_6H_4)C≡C]Ru(η^2-dppe)$_2$Cl (**2**; 0.250 g, 0.152 mmol), 4-nitrophenylacetylene (0.089 g, 0.608 mmol), and KPF_6 (0.084 g, 0.456 mmol) were dissolved in 30 mL of dichloromethane and the mixture was stirred for 2 days at room temperature. After removal of the solvent, the red residue was dissolved in THF in the presence of excess KO^{t}Bu (0.034 g, 0.304 mmol) and stirred for 2 h. After evacuation of the solvent, the product was chromatographed through an alumina column using toluene as eluant. The fraction containing the product was then concentrated to dryness and the residual solid washed with *n*-pentane (3 × 5 mL) to afford the desired red complex **5** (0.130 g, 0.074 mmol, 49%). Anal. Calcd for $C_{106}H_{95}FeNO_2P_6Ru$: C, 72.43; H, 5.45. Found: C, 73.19; H, 5.85. MS (ESI): *m*/*z* 1757.4182 ($M^{\bullet+}$), calcd for $C_{106}H_{95}FeNO_2P_6Ru$ 1757.4263 ($M^{\bullet+}$). FT-IR (ν, KBr, cm^{-1}): 2070 (sh), 2044 (FeC≡C and RuC≡C's). ^{31}P NMR (81 MHz, C_6D_6, δ in ppm): 101.7 (s, 2P, (dppe)Fe), 54.6 (s, 4P, (dppe)$_2$Ru). ^{1}H NMR (200 MHz, C_6D_6, δ in ppm): 8.12 (m, 6H, H_{Ar}), 7.89 (m, 8H, J = 6 Hz, H_{Ar}), 7.40–6.74 (m, 52H, H_{Ar}), 6.62 (d, 2H, J = 8.4 Hz, H_{Ar}), 2.84 (m, 2H, CH_2), 2.52 (m, 8H, CH_2), 1.99 (m, 2H, CH_2), 1.59 (s, 15H, $C_5(CH_3)_5$). ^{13}C{^{1}H} NMR (125 MHz, C_6D_6, δ in ppm): 154.6 (q, $^2J_{CP}$ = 14.4 Hz, Ru*C*≡C), 144.1 (s, C_{Ar}), 140.6–137.0 (m, $C_{Ar/dppe}$ + Fe*C*≡C), 135.8–135.0 (m, *C*H$_{Ar/dppe}$ + C_{Ar}), 131.0–128.1 (m, *C*H$_{Ar/dppe}$ + *C*H$_{Ar}$ + Ru*C*≡C), 126.2, 124.3, 121.8, 120.6, 119.4 (s, C_{Ar} and MC≡*C*'s), 88.5 (s, $C_5(CH_3)_5$), 32.4 and 31.9 (m, $(CH_2)_{dppe/Ru\&Fe}$), 11.2 (s, $C_5(CH_3)_5$). CV (CH_2Cl_2, 0.1 M *n*-$Bu_4N^+PF_6^-$, 20 °C, 0.1 V s^{-1}; $E°$ in V vs SCE (ΔE_p in V, $i_{p,a}/i_{p,c}$)): −1.25 (0.14, 1.0), −0.23 (0.07, 1.0), 0.50 (0.07, 1.0).

Synthesis of [(η^2-dppe)(η^5-C_5Me_5)Fe[C≡C-1,4-(C_6H_4)C≡C]-Ru(η^2-dppe)$_2${C≡C(4-$C_6H_4NO_2$)}][PF_6] (5[PF_6]). [(η^5-$C_5H_5)_2$Fe]-[PF_6] (0.024 g; 0.074 mmol) was added to a solution of **5** (0.130 g, 0.074 mmol) in dichloromethane. Stirring was maintained for 2 h at 20 °C, and the solution was concentrated in vacuo. Addition of diethyl ether resulted in the precipitation of **5**[PF_6], which could be isolated (0.120 g, 0.063 mmol, 85%) after successive washings with toluene (5 mL), diethyl ether (5 mL), and *n*-pentane (5 mL). FT-IR (ν, KBr/CH_2Cl_2, cm^{-1}): 2037/2045 (s, RuC≡C), 1945/1950 (s, FeC≡C). ^{31}P NMR (81 MHz, CD_2Cl_2, δ in ppm): 135.2 (broad s, P, Ru(dppe)$_2$). ^{1}H NMR (500 MHz, CD_2Cl_2, δ in ppm, numbering according to Figure 2): 31.5 (s, 2H, H_2), 9.1 (broad s, 2H, H_9), 8.3–5.7 (m, 56H, $H_{Ar/dppe}$), 4.2 (s, 4H, H_6 or H_7), 3.6 (s, 4H, H_6 or H_7), 2.7 (s, 8H, $(H_2)_{dppe/Ru}$), −3.8 (s, 2H, H_{10}), −9.4 (s, 15H, H_{11}), −65.6 (s, 2H, H_1).

Synthesis of Cl(η^2-dppe)$_2$RuC≡C(3-C_6H_4F)] (11). In a Schlenk tube, [RuCl(dppe)$_2$][OTf] (**7**; 0.160 g, 0.148 mmol) and HC≡C(3-C_6H_4F) (0.20 mL, 1.48 mmol) were dissolved in 10 mL of dichloromethane. The brown-orange solution was stirred for 2 days at room temperature, and the solvent was removed in vacuo. The remaining brownish solid was washed twice with diethyl ether (2 × 3 mL), extracted with dichloromethane (2 × 5 mL), and filtered through paper. Subsequently, ca. 3 mL of NEt_3 was added and the solution was stirred for a further 2 h at 25 °C. After removal of the

(46) Greenwood, N. N. *Mössbauer Spectroscopy*; Chapman and Hall: London, 1971.

Table 5. Crystal Data, Data Collection, and Refinement Parameters for 11·2CH$_2$Cl$_2$

formula	$C_{60}H_{52}ClFP_4Ru \cdot 2CH_2Cl_2$
fw	1222.27
temp (K)	100(2)
cryst syst	monoclinic
space group	$P2_1/n$
a (Å)	14.0228(16)
b(Å)	17.5293(17)
α (deg)	90.0
β (deg)	100.962(7)
γ (deg)	90.0
V (Å^3)	5665.8(10)
Z	4
D_{calcd} (g cm^{-3})	1.433
cryst size (mm)	0.55 × 0.25 × 0.05
F(000)	2504
abs coeff (mm^{-1})	0.669
θ range (deg)	2.92–27.40
hkl range	−17 to +18, −22 to +22, −30 to +29
no. of reflns: total/unique	43 235/12 775
R(int)	0.0869
no. of restraints/params	0/658
final R	0.0846
R_w	0.1883
R indices (all data)	0.1362
R_w (all data)	0.2149
goodness of fit/F^2 (S_w)	1.035
$\Delta\rho_{max}$ (e Å^{-3})	2.186
$\Delta\rho_{min}$ (e Å^{-3})	−2.263

solvent and extraction with CH_2Cl_2, the pale orange solution was chromatographed on Al_2O_3 (neutral grade), using CH_2Cl_2 as eluant. The desired complex **11** was eluted as a yellow band, affording a pale yellow solid (0.095 g, 0.09 mmol; 61%). Anal. Calcd for $C_{60}H_{52}ClFP_4Ru$: C, 68.47; H, 4.98; F, 1.81. Found: C, 68.11; H, 4.99; F, 1.94. MS (ESI): m/z 1052.1799 ($M^{\bullet+}$), calcd for $C_{60}H_{52}ClFP_4Ru$ 1052.1749 ($M^{\bullet+}$). FT-IR (ν, KBr/CH_2Cl_2, cm^{-1}): 2057/2065 (RuC≡C). ^{31}P NMR (81 MHz, $CDCl_3$, δ in ppm): 50.7 (s, dppe). ^{19}F NMR (188 MHz, $CDCl_3$, δ in ppm): −116.1 (s, F_{Ar}). ^{1}H NMR (200 MHz, $CDCl_3$, δ in ppm): 7.50 (m, 8H, $H_{Ar/dppe}$), 7.35–6.95 (m, 33H, H_{Ar}), 6.70 (m, 1H, H_{Ar}), 6.45 (m, 1H, H_{Ar}), 6.25 (m, 1H, H_{Ar}), 2.71 (m, 8H, (CH_2)$_{dppe}$). ^{13}C{^{1}H} NMR (125 MHz, $CDCl_3$, δ in ppm): 163.3 (d, $^1J_{CF}$ = 243 Hz, CF), 137.0 and 136.3 (2 × m, $C_{Ar/dppe}$), 135.1 and 134.9 (2 × s, $C_{Ar/dppe}$), 132.6 (d, $^3J_{CF}$ = 9.7 Hz, C_{Ar}), 129.6 and 129.5 (2 × s, $C_{para/dppe}$), 129.1 (d, $^3J_{CF}$ = 9.3 Hz, CH_{Ar}), 127.9 and 127.6 (2 × s, $C_{Ar/dppe}$), 120.3 (q, $^2J_{CP}$ = 15.4 Hz, RuC≡C), 117.1 (d, $^2J_{CF}$ = 20.7 Hz, CH_{Ar}), 113.4 (s, RuC≡C), 110.4 (d, $^2J_{CF}$ = 21.4 Hz, CH_{Ar}), 31.3 (m, (CH_2)$_{dppe}$). UV–vis (λ_{max}, nm (10^{-3} ϵ, M^{-1}cm^{-1}); CH_2Cl_2): 328 (14.0). CV (CH_2Cl_2, 0.1 M n-$Bu_4N^+PF_6^-$, 20 °C, 0.1 V s^{-1}; $E°$ in V vs SCE (ΔE_p in V, $i_{p,c}/i_{p,a}$)): 1.37 (0.148, 0.45), 0.51 (0.072, 1.0).

Crystallography. Data collection of crystals of **11**·2CH$_2$Cl$_2$ was performed on an APEXII Bruker-AXS diffractometer (see Table 5 for details). The structure was solved by direct methods using the SIR97 program[47] and then refined with full-matrix least-squares methods based on F^2 (SHELX-97)[48] with the aid of the WINGX program.[49] All non-hydrogen atoms were refined with anisotropic thermal parameters. H atoms were included in their calculated positions. A final refinement on F^2 with 12 775 unique intensities and 658 parameters converged at $R_w(F^2) = 0.1883$ ($R(F) = 0.0846$) for 8075 observed reflections with $I > 2\sigma(I)$. Selected bond lengths and angles are given in Table 6.

Table 6. Selected Bond Lengths (Å) and Angles (deg) for 11·2CH$_2$Cl$_2$

Selected Bond Lengths	
Ru−P1A	2.3947(17)
Ru−P2A	2.3689(16)
Ru−P1B	2.3852(16)
Ru–P2B	2.3562(16)
Ru1−Cl	2.5370(18)
Ru1−C1	2.043(8)
C1−C2	1.096(9)
C2−C3	1.524(11)
C3−C4	1.383(11)
C4−C5	1.379(13)
C5−C6	1.373(15)
C6−C7	1.342(14)
C7−C8	1.383(13)
C8−C3	1.430(12)
C7−F7	1.434(12)
Selected Bond and Dihedral Angles	
P1A−Ru1−P2A	82.54(6)
P1B−Ru1−P2B	82.38(6)
P1A−Ru1−C1	92.48(17)
Cl−Ru1−C1	175.52(17)
P2A− Ru1−C1	90.10(16)
Ru1−C1−C2	176.7(6)
C1−C2−C3	172.7(7)
C2−C3−C4	123.1(8)
C4−C5−C6	121.3(10)
C6−C7−C8	123.7(10)
C6−C7−F7	118.9(9)
P1A−Ru1/C3−C4[a]	148.2
P2B−Ru1/C3−C4[a]	48.6

[a] Dihedral angle.

Determination of the ESPs of the "(C≡C)Ru(η^2-dppe)$_2$Cl" End Group. Pure samples of **9-F** and **11** (ca. 0.05 mmol) were each dissolved in 1 mL of freshly distilled and deoxygenated CCl_4. These solutions were transferred to NMR tubes under argon, and 5 μL (0.076 mmol) of fluorobenzene was syringed in each tube as internal reference. After homogenization of the solution, the ^{19}F{^{1}H} NMR spectra of both samples were recorded at 25 °C. The values of σ_I and σ_R, as well as the σ_p values, were then derived using the appropriate equations.[50]

Acknowledgment. M.G.H. thanks the Australian Research Council for financial support and an ARC Australian Professorial Fellowship. F.P. and N.G. thank the CNRS for financial support and Region Bretagne for a Ph.D. grant. A. Mari (LCC, Toulouse), A. Bondon (PRISM, UMR CNRS 6026), and S. Sinbandhit (CRMPO, Rennes) are acknowledged for their assistance in recording the Mössbauer and the NMR spectra.

Supporting Information Available: A CIF file giving crystal data for **11**·2CH$_2$Cl$_2$. This material is available free of charge via the Internet at http://pubs.acs.org. Final atomic positional coordinates, with estimated standard deviations, bond lengths and angles, and anisotropic thermal parameters, have been deposited at the Cambridge Crystallographic Data Centre and allocated the deposition number CCDC 668838.

OM700584M

(47) Altomare, A.; Burla, M. C.; Camalli, M.; Cascarano, G.; Giacovazzo, C.; Guagliardi, A.; Moliterni, A. G. G.; Polidori, G.; Spagna, R. *J. Appl. Crystallogr.* **1999**, *32*, 115–119.

(48) Sheldrick, G. M. *SHELX97-2: Program for the refinement of crystal structures*; University of Göttingen, Göttingen, Germany, 1997.

(49) Farrugia, L. J. *J. Appl. Crystallogr.* **1999**, *32*, 837–838.

(50) Hansch, C.; Leo, A.; Taft, R. W. *Chem. Rev.* **1991**, *91*, 165–195.